ACS OMEGA

Open Access

http://pubs.acs.org/journal/acsodf

Article

Controllable Fabrication of Hydrophilic Surface Micro/Nanostructures of CFRP by Femtosecond Laser

Pei Zuo, Tongfeng Liu, Fang Li, Guoyan Wang, Kaihu Zhang, Xin Li, Weina Han, Hong Tian, Lifei Hu, Helang Huang, Di Zhu, and Lan Jiang*

Cite This: *ACS Omega* 2024, 9, 20988−20996

Read Online

ACCESS | Metrics & More | Article Recommendations | Supporting Information

ABSTRACT: Carbon fiber reinforced polymer (CFRP), a highly engineered lightweight material with superior properties, is widely used in industrial fields, such as aerospace, automobile, and railway transportation, as well as medical implants and supercapacitor. This work presents an effective surface treatment method for the controllable fabrication of hydrophilic surface micro/nanostructures of CFRP through femtosecond laser processing. Selective removal of the epoxy resin and leaving the carbon fibers exposed are achieved when CFRP is weakly ablated by a femtosecond laser. The diameters and structures of the carbon fibers can be controlled by adjusting the laser processing parameters. Three-dimensional surface micro/nanostructures are processed when CFRP is strongly ablated by a femtosecond laser. Meanwhile, the transformation of the sp^2 orbitals to sp^3 orbitals of graphitic carbons of carbon fibers is induced by a femtosecond laser. Moreover, the investigation of surface roughness and wettability of femtosecond laser-processed CFRP indicates increased roughness and excellent hydrophilicity (a contact angle of 28.1°). This work reveals the effect of femtosecond laser processing on the regulation of the physicochemical properties of CFRP, which can be applicable to surface treatment and performance control of other fiber-resin composites. The excellent hydrophilicity will be conducive to the combination of CFRP with other materials or to reducing the friction resistance of CFRP used in medical implants.

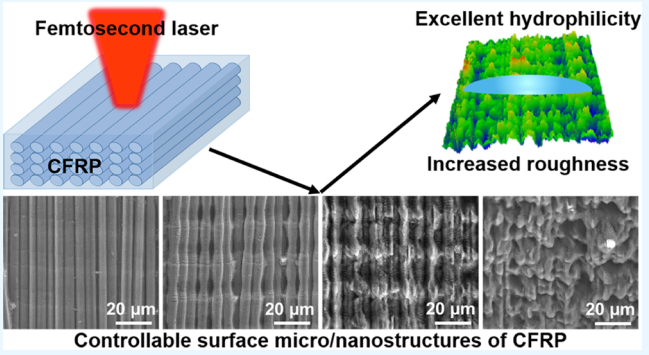

INTRODUCTION

Carbon fiber reinforced polymer (CFRP) is a kind of highly engineered material that offers high specific modulus and high specific strength.[1] CFRP has superior mechanical, thermal, and chemical properties, and is a kind of ideal lightweight material.[2,3] CFRP is widely used in the main, functional, protective, and auxiliary components of various types of space vehicles in the aerospace industry.[3,4] It may be the route one must take to the development trend of high bearing capacity, high stability, long life, energy saving, and emission reduction in automobiles, railway transportation, national defense, and other industrial fields.[1,5] In addition, CFRP has been used in medical implants[6−10] and composite structural supercapacitors.[11−13] In the above industrial, medical, or supercapacitor applications, CFRP needs not only to be cut and drilled[14−16] but also to be surface-treated.[17−24] This may be due to the intrinsic surface hydrophobicity of CFRP, which leads to low bonding strength when used in combination with other materials or produces large friction resistance in close contact with human tissue. Hence, it is urgent and challenging to develop a simple, effective, controllable, and high-precision surface treatment strategy for CFRP.

Currently, the surface treatment of carbon fiber composites includes surface chemical modification, removal of the surface weak boundary layer, improved wetting of the low-energy surface, and increased surface roughness, which can enlarge the bondable surface area or improve the mechanical interlocking.[21−23,25] Surface chemical modification can be achieved by grafting multiwalled carbon nanotubes (MWCNTs) onto a carbon fiber surface using silane coupling agent as carrier.[23] Removal of the surface weak boundary layer can be achieved through UV or picosecond laser cleaning.[22,26] Improving the wetting of low-energy surface and increasing the surface roughness of carbon fiber composites can be achieved through mechanical methods (such as manual hand sanding, grit blasting, and peel-ply plus grit blasting)[21,27] and energetic techniques, such as plasma treatment[21,27−31] and laser processing.[24,32−35] Among them, the mechanical method had

Received: January 5, 2024
Revised: February 21, 2024
Accepted: April 16, 2024
Published: May 3, 2024

the advantage of low cost, but its flexibility, adjustability, efficiency, and precision were relatively low. Plasma treatment has the advantage of relatively high efficiency and precision, but it needs a special atmosphere environment and inorganic or organic masks; the treatment effect is time-sensitive; the treatment process is relatively complex, and not flexible enough; and the equipment is generally expensive. Laser surface processing can achieve surface modification, surface etching, and micro/nanostructure processing of materials and has many advantages, such as simple operation, no special environment required, maskless, arbitrary patterning, high flexibility, and high controllability. Moreover, a femtosecond laser with ultrahigh power density and ultrashort pulse width has a nonlinear nonequilibrium processing feature, and nonthermal processing effects. Hence, femtosecond laser surface processing also has the advantages of high efficiency and high precision[36−39] and should be an ideal strategy for the surface treatment of materials.[17−20,40]

In this work, we proposed a surface treatment method to controllably fabricate the hydrophilic surface micro/nanostructures of CFRP through femtosecond laser processing. Selective removal of the epoxy resin and leaving the carbon fibers exposed were achieved when CFRP was weakly ablated by a femtosecond laser. The dependence of the diameters and structures of carbon fibers on laser pulse energy and scanning speed was investigated. Three-dimensional micro/nanostructures of CFRP were processed when CFRP was strongly ablated by a femtosecond laser. Characterization analyses indicated lattice destruction of carbon fibers, transformation of sp^2 orbitals to sp^3 orbitals of the graphitic carbons of carbon fibers, and photo-oxidation of phenyl groups of epoxy resin induced by a femtosecond laser. To investigate the surface properties and functions of femtosecond laser-processed CFRP, the roughness of laser-processed CFRP with typical surface structures and the surface wettability of CFRP processed by femtosecond laser with different parameters were investigated, indicating increased roughness and excellent hydrophilicity of laser-processed CFRP. This work systematically revealed the effect of femtosecond laser processing on the regulation of the physicochemical properties of CFRP, which can be applicable to the surface treatment and performance control of other fiber-resin composites. The excellent hydrophilicity of laser-processed CFRP is conducive to enhancing the bonding strength and adhesion of CFRP used in combination with other materials to better meet the mechanical strength requirements of CFRP-based components in the fields, such as significant aerospace and automotive industries. It also reduces the friction resistance of CFRP in close contact with human tissue to better meet the use of medical implants.

RESULTS AND DISCUSSION

In this work, the CFRP used (Figure S1) consisted of carbon fiber and epoxy resin. It was fabricated through the material preparation process: first, a single layer of carbon fiber and resin glue were mixed into a single-layer structure with thickness of ∼0.8 mm; then, multiple single-layer structures were laminated and solidified to form the final CFRP structure. The carbon fibers in each layer were distributed in parallel and periodically arranged (Figure 1a), and the average diameter of the carbon fibers was ∼5.5 μm (the measurement method is shown in Figure S2). The most surface layer of CFRP was epoxy resin, and the roughness was 0.03 μm (Figure 1b).

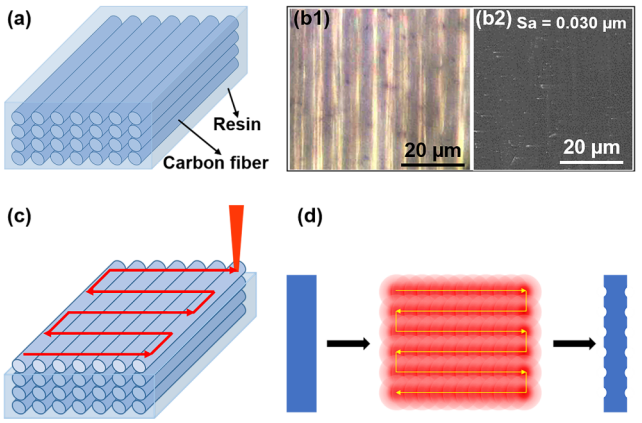

Figure 1. (a) Structure diagram of CFRP. (b) Optical and SEM images of the used CFRP. (c) Schematic diagram of laser processing of CFRP. (d) Diagram of the processing effect of the laser scanning direction perpendicular to the carbon fiber.

Femtosecond laser pulses were focused on the surface of CFRP, and their scanning direction was perpendicular to the direction of the carbon fibers during laser processing of CFRP for surface etching and micro/nanostructure fabrication (Figure 1c). Figure 1d shows a diagram of the processing effect of the laser scanning direction perpendicular to the carbon fiber, which can reveal the basic bamboo-like structures of the exposed carbon fiber. Surface etching can selectively remove the epoxy resin at the selected location and expose the carbon fibers (Figure S3). Flocculent structures of the epoxy resin on the CFRP surface were revealed when laser processing was not enough to etch the resin away but to process its surface (Figure S4).

Surface Structure Regulation of CFRP Processed by a Femtosecond Laser. Femtosecond laser surface processing can achieve selective removal of the epoxy resin, leaving the carbon fibers exposed. As shown in Figure 2, with the increase

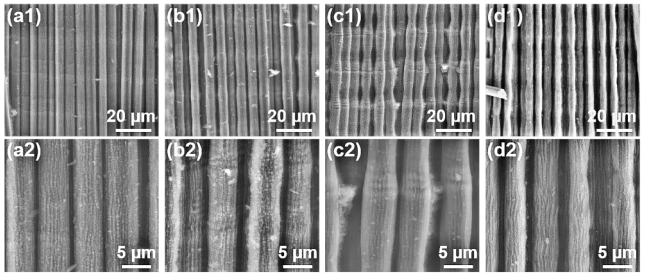

Figure 2. Morphology (SEM images) of exposed carbon fibers after the epoxy resin was selectively removed by a femtosecond laser with laser pulse energies of (a) 1 μJ, (b) 4 μJ, (c) 7 μJ, and (d) 12 μJ. The laser scanning speed was 1000 μm/s.

of laser pulse energy, the diameter of carbon fibers decreased (Figure 2a1-d1), indicating that, except for the removal of epoxy resin, carbon fibers were also ablated and the ablation was gradually enhanced, resulting in more material removal of carbon fibers. At the same time, carbon fibers showed bamboo-like structures, which became increasingly visible with the increase of laser pulse energy. The length of "bamboo" was ∼22 μm, about twice the laser scanning spacing, which can be attributed to the following speculation. In the laser line-scanning process, the scanning direction was perpendicular to

https://doi.org/10.1021/acsomega.4c00148
ACS Omega 2024, 9, 20988−20996

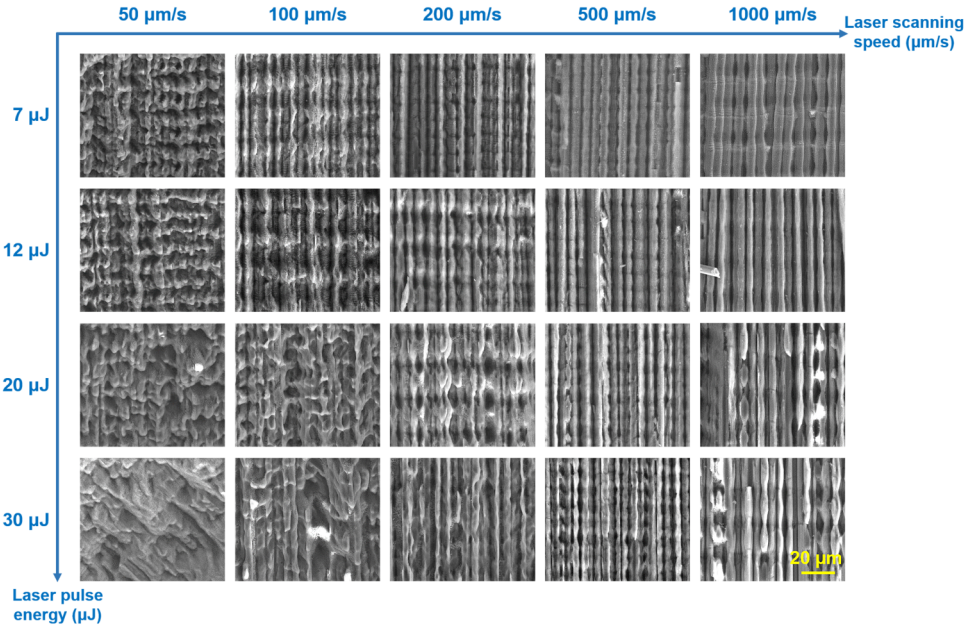

Figure 3. Morphology (SEM images) of the CFRP processed by a femtosecond laser with different laser pulse energies and scanning speeds.

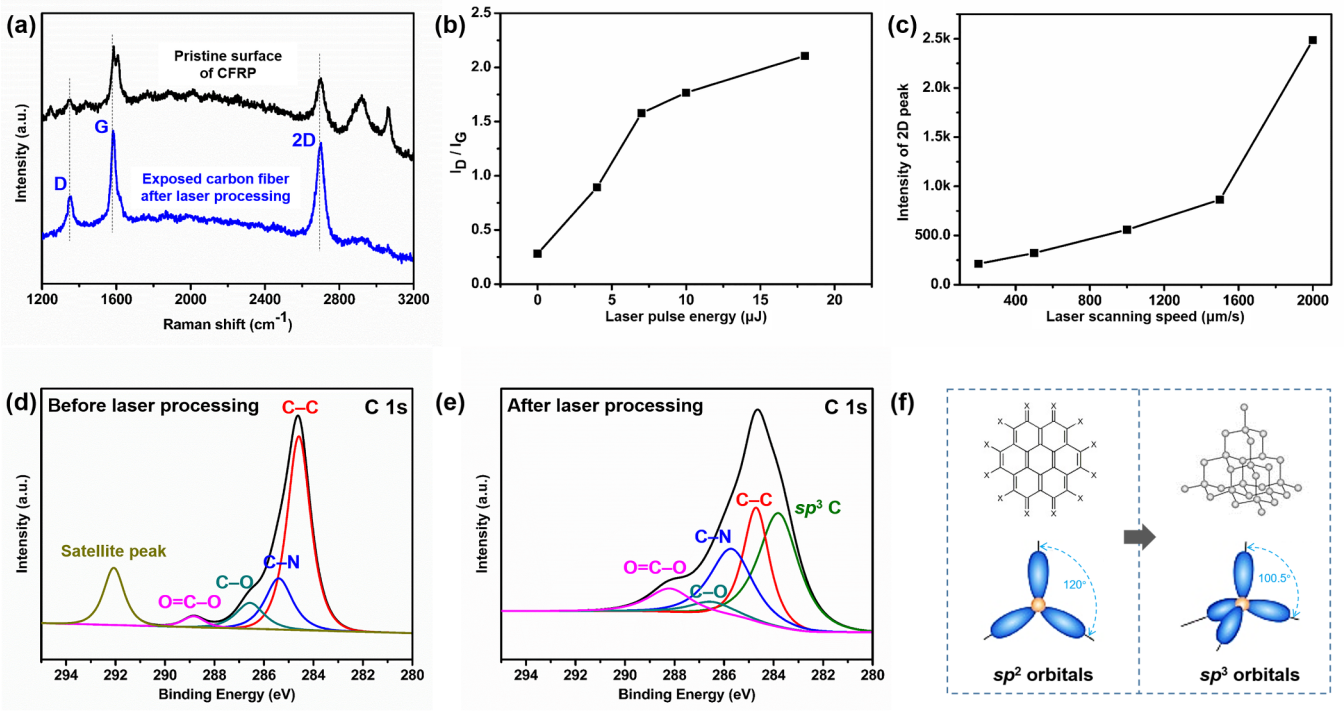

Figure 4. Characterization of the change of surface composition of CFRP processed by a femtosecond laser. (a) Raman spectra of the pristine surface of CFRP and the exposed carbon fiber after femtosecond laser processing. (b) Dependence of the ratio of the intensities of the D-peak and G-peak (I_D/I_G) on the laser pulse energy (laser scan speed was 100 μm/s). (c) Dependence of the intensity of the 2D-peak on the laser scanning speed (laser pulse energy was 10 μJ). XPS C 1s spectra of CFRP (d) before and (e) after femtosecond laser processing. (f) sp^2 orbitals of graphitic carbon of carbon fiber and sp^3 orbital of diamond-like lattice.

the direction of the carbon fibers. After the first line of scanning processing, the epoxy resin was removed, then the laser pulse energy was directly deposited on the carbon fibers in the second line of scanning processing, resulting in relatively strong ablation of the carbon fibers. With laser progressive scanning processing, this process occurred alternately. When the laser pulse energy was too large, for example, greater than 20 μJ, the carbon fibers were strongly ablated, became section by section, and were even broken (Figure S5). The decreasing diameter and more visible bamboo-like structure of carbon fibers with increasing laser pulse energy are simplistically explained in Figures S6,S7. In addition, the surface of the carbon fibers was also modified or processed, and the nanoburrs and periodic structures were created on the carbon fiber surface. With the increase of laser pulse energy, nanoburrs-periodic structures (Figure 2a2−b2) and periodic

https://doi.org/10.1021/acsomega.4c00148
ACS Omega 2024, 9, 20988−20996

structures (Figure 2c2−d2) were created on the carbon fiber surface, and the period of periodic structures was ∼680 nm. According to electromagnetic theory, the formation of a laser-induced periodic surface structure (LIPSS) on the carbon fiber surface is attributed to the generation of a surface plasmon polariton (SPP) propagating parallel to the surface, interference between the incident light wave and the SPP wave to modulate light intensity, and imprinting of the interference pattern on the carbon fiber surface.[41,42]

Except that the surface epoxy resin was completely removed, the surface micro/nanostructures, the main composition of which was carbon fibers, were fabricated when the laser pulse energy was high or the scanning speed was low in the process of femtosecond laser processing. Figure 3 shows the morphology of CFRP processed by femtosecond laser processing with different laser pulse energies and scanning speeds. When the scanning speed was low, except the surface epoxy resin was completely removed, the carbon fibers were ablated and melted and the heat accumulation effect was strong. When the scanning speed was high, the removal of epoxy resin was mainly realized, and the thermal melting effect was weak. With the increase of laser pulse energy, carbon fibers were more strongly ablated and interrupted, the thermal melting effect was enhanced, multiple carbon fibers melted together, and no single carbon fiber was visible. In addition, the dependence of the diameters of the processed carbon fibers on the laser pulse energy and scanning speed was also investigated, as shown in Figures S8 and S9. With the increase of laser pulse energy from 0−30 μJ (laser scanning speed was 1000 μm/s), the diameters of the processed carbon fibers decreased gradually. With the increase of scanning speed from 100−1000 μm/s (laser pulse energy was 7 μJ), the diameters of the processed carbon fibers increased gradually. With the decrease of laser scanning speed, the bamboo-like structures of carbon fibers became dense, and the length of "bamboos" was ∼11 μm, about the scanning spacing. This was speculatively attributed to the fact that when the laser scanning speed decreased, the pulse numbers per unit area increased, leading to the increase of deposited laser energy and the strong incubation effect, resulting in the strong ablation of carbon fibers in every line of femtosecond laser scanning processing. The "bamboos" were interrupted when the carbon fibers were strongly ablated at too high laser pulse energy or too low scanning speed, and the surface of laser-processed CFRP revealed three-dimensional micronano structures.

Surface Composition Analysis of Femtosecond Laser-Processed CFRP. To characterize the change in surface composition of CFRP processed by a femtosecond laser, Raman and X-ray photoelectron spectroscopy (XPS) spectra were obtained. Figure 4a shows the Raman spectra of the pristine surface of CFRP and the exposed carbon fiber after femtosecond laser processing. The Raman spectrum of pristine CFRP surface shows seven Raman modes. The Raman frequencies (cm^{-1}) and assignments of the Raman modes are shown in Table S1, which indicates the atomic vibration characteristics of epoxy resin and carbon fiber. The Raman spectrum of the exposed carbon fiber after femtosecond laser processing shows three Raman modes at 1347, 1585, and 2700 cm^{-1}, respectively, assigned to the D-peak, G-peak, and 2D-peak. The D-peak was a disorder-induced peak and corresponded to the disordered graphitic lattice (A_{1g} symmetry), which was attributed to the reduced symmetry of the graphite lattice near edges (sp^3 carbon atoms).[43,44] The G-peak corresponded to the ideal graphitic lattice (E_{2g} symmetry), which was attributed to the in-plane vibration of the sp^2 carbon atoms.[43,44] The 2D-peak was attributed to the first overtone of the D-peak, and could reflect the degree of perfection of the graphite lamellar structure.[44,45] The ratio of the intensities of the D-peak and G-peak, I_D/I_G, has been widely utilized to characterize the degree of structural disorder.[43] In the process of femtosecond laser processing CFRP, the ratio of the intensities of the D-peak and G-peak (I_D/I_G) increased with the increase of the laser pulse energy, as shown in Figure 4b, which indicated the increase of the degree of structural disorder. This was attributed to the stronger ablation and lattice destruction of carbon fibers, namely, more carbon bond breaking and the appearance of more sp^3 carbon atoms, when CFRP was processed by femtosecond laser with high laser pulse energy. In addition, the intensity of the 2D-peak was positively correlated with the laser scanning speed, as shown in Figure 4c. This indicated the decrease of the degree of perfection of the graphite lamellar structure with the decrease of laser scanning speed, which means stronger ablation. The results of Raman characterization were consistent with the phenomenon of morphological characterization of CFRP processed by a femtosecond laser.

XPS spectra were obtained to characterize the valence state of CFRP before and after femtosecond laser processing. Figure 4d shows the C 1s spectrum of CFRP before femtosecond laser processing, which discloses five split peaks. The binding energies from low to high were assigned to C−C groups (∼284.6 eV), C−N groups (∼285.5 eV), C−O groups (∼286.6 eV), O−C = O groups (∼288.5 eV), and a satellite peak due to $\pi-\pi^*$ transition (∼292.1 eV).[46−52] Figure 4e shows the C 1s spectra of CFRP after femtosecond laser processing, which discloses five split peaks. The binding energies from low to high were assigned to sp^3 carbons (∼283.8 eV), C−C groups (∼284.6 eV), C−N groups (∼285.5 eV), C−O groups (∼286.6 eV), and O−C = O groups (∼288.5 eV).[46−51,53] The sp^3 carbons might be related to the diamond lattice, which indicated the transformation of sp^2 orbitals to sp^3 orbitals of the graphitic carbons of carbon fibers induced by the femtosecond laser (Figure 4f),[53,54] consistent with the result revealed by Raman characterization. In addition, Figure 4e had no satellite peak due to $\pi-\pi^*$ transition shown in Figure 4d, and the disappearance of the C 1s satellite peak, which is the characteristic of surface-tethered aromatic species, indicated the photo-oxidation of the phenyl groups of epoxy resin processed by femtosecond laser.[55,56]

Roughness and Wettability of Femtosecond Laser-Processed CFRP. To investigate the surface properties of femtosecond laser-processed CFRP, the surface roughness (Sa, the arithmetic average height) of laser-processed CFRP with typical surface structures was tested by a 3D laser confocal microscope (Figure 5). The surface of the nontreated CFRP was solidified epoxy resin, which was relatively smooth, and the Sa was 0.03 μm (Figure 1b). The Sas of laser-processed CFRP, the surfaces of which were complete carbon fibers, carbon fibers with sparse bamboo-like structures, carbon fibers with compact bamboo-like structures, and fractured carbon fibers, were 2.020, 1.678, 1.278, and 1.592 μm, respectively (Figure 5a−d). As the laser ablation further became stronger, the surface of the processed CFRP revealed three-dimensional microstructures and became rougher with larger roughnesses, such as 1.702 and 2.267 μm (Figure 5e,f). The larger roughness of laser-processed CFRP than that of nonprocessed

https://doi.org/10.1021/acsomega.4c00148
ACS Omega 2024, 9, 20988−20996

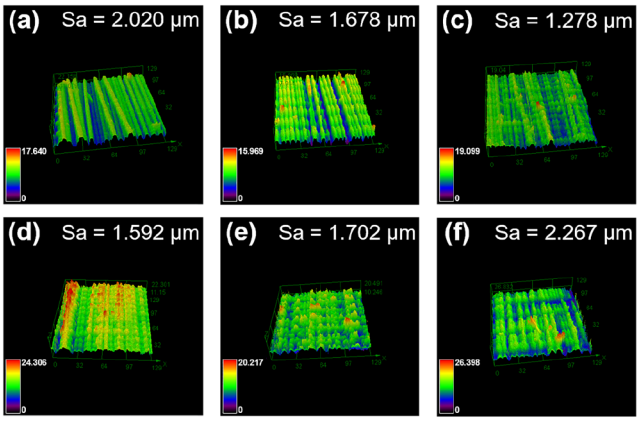

Figure 5. Sa of CFRP with typical surface structures processed by a femtosecond laser. Sa of laser-processed CFRP with surface structures of (a) complete carbon fibers; (b) carbon fibers with sparse bamboo-like structures; (c) carbon fibers with compact bamboo-like structures; (d) fractured carbon fibers; (e) small three-dimensional microstructures; and (f) large three-dimensional microstructures. The dimension of the tested area was 129 × 129 μm^2.

CFRP was mainly attributed to the selective removal of resin and the exposure of carbon fibers, which was due to the smaller ablation threshold and large ablation removal rate of resin than that of carbon fiber. The arranged carbon fibers had curved structures, leading to greater roughness than the flat resin. As the diameter of the carbon fibers decreased, the curved structures decreased and the roughness decreased. With the fracture of carbon fibers, the three-dimensional surface structures were formed gradually, and the roughness increased gradually. In addition, the more complete parameters of surface roughness of the laser-processed CFRP with typical surface structures shown in Figure 5 are shown in Table S2, including root-mean-square height (Sq), degree of skewness (Ssk), kurtosis (Sku), maximum peak height (Sp), maximum valley depth (Sv), maximum height (Sz), and arithmetic average height (Sa). They exhibited a roughness contrast similar to Sa.

To investigate the physical function of the laser-processed CFRP, we also investigated surface wettability. Unique wetting phenomena, such as excellent hydrophobicity and hydrophilicity, can be exhibited by superwettable textured surfaces and have enabled a wide variety of applications in the fields of bionics, biosensing, surface performance improvement, and so on.[57−62] Ultrafast laser processing has great potential in regulating the surface wettability of various materials and achieved significant applications.[57−60,63−65] The surface wettability of CFRP processed by a femtosecond laser with different laser pulse energies and scanning speeds is shown in Figure 6. The nontreated CFRP was hydrophobic, and its initial contact angle of water droplet was 105.6°, which was attributed to the good hydrophobicity of smooth epoxy resin on the surface of nontreated CFRP.[66−68] Figure 6a shows the dependence of the droplet contact angle of the laser-processed CFRP on laser scanning speed. It revealed that the droplet contact angle of the laser-processed CFRP decreased with the decrease of laser scanning speed, and the rate of decrease was gradually slowing down. When the laser scanning speed was reduced to 200 μm/s, the contact angle was as small as 36.5°, indicating the good hydrophilicity of laser-processed CFRP. Figure 6b shows the dependence of the droplet contact angle of laser-processed CFRP on laser pulse energy. It revealed that with the decrease of laser pulse energy, the droplet contact angle of laser-processed CFRP first decreased rapidly, then decreased slowly, and finally remained unchanged. When the laser pulse energy was increased to 50 μJ, the contact angle reached 28.1°, which indicated better hydrophilicity of the laser-processed CFRP. In addition, the wettability of the laser-processed CFRP was also compared with that of surface-treated CFRP by different methods reported in the literature, as shown in Table S3. It revealed the excellent hydrophilicity of the femtosecond laser-processed CFRP. In addition, the wettability of CFRP controlled by femtosecond laser processing can not only achieve hydrophilicity but also achieve hydrophobicity.[69−72] This may be attributed to the different laser processing parameters, as well as the different resin composition, resin-fiber composition ratio, carbon fiber arrangement structure, fiber layer spacing, etc., which will affect the results of femtosecond laser processing. The excellent hydrophilicity of the laser-processed CFRP can be speculatively attributed to the intrinsic hydrophilicity of exposed carbon fibers,[73,74] the transformation of sp^2 orbitals to sp^3 orbitals of carbons, which can lead to more elevated free energy,[75,76] and the carbon fiber-epoxy resin fused micro/nanostructures, which may be beneficial to the capillary effect of water droplets.[77−79] The excellent hydrophilicity of laser-processed CFRP should be conducive to enhancing the

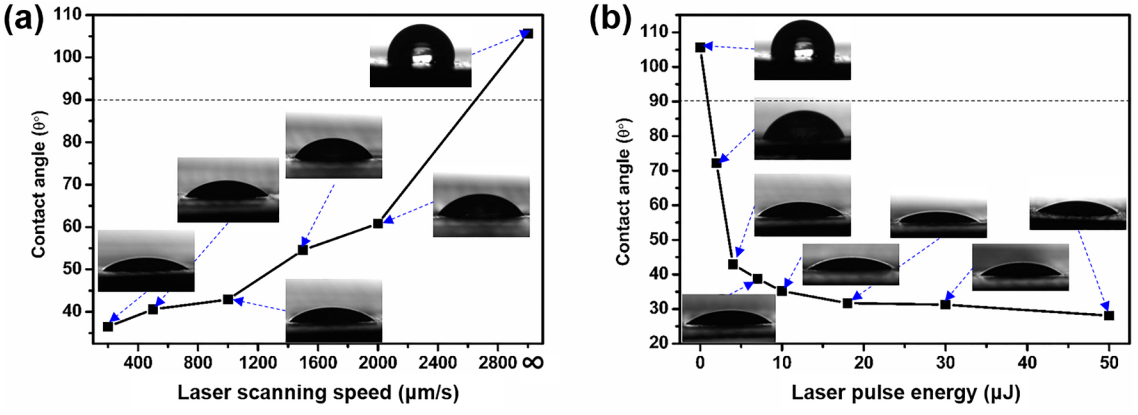

Figure 6. Surface wettability of CFRP processed by a femtosecond laser with different parameters. (a) Dependence of the droplet contact angle of the laser-processed CFRP on (a) laser scanning speed (laser pulse energy was 7 μJ) and (b) laser pulse energy (laser scanning speed was 500 μm/s).

https://doi.org/10.1021/acsomega.4c00148
ACS Omega 2024, 9, 20988−20996

bonding strength of CFRP used in combination with other materials or reducing the friction resistance of CFRP in close contact with human tissue, hence better meeting the usage requirements of CFRP.

CONCLUSIONS

An effective surface treatment method was proposed to controllably fabricate the hydrophilic surface micro/nanostructures of CFRP through femtosecond laser processing. Selective removal of the epoxy resin and leaving the carbon fibers exposed were achieved by weak femtosecond laser ablation. The dependence of the diameters and structures of the carbon fibers on the laser pulse energy and scanning speed were investigated, and the three-dimensional micro/nanostructures of CFRP were processed by strong femtosecond laser ablation. Raman and XPS characterization analysis indicated the lattice destruction of carbon fibers, the transformation of sp^2 orbitals to sp^3 orbitals of the graphitic carbons of carbon fibers, and the photo-oxidation of phenyl groups of epoxy resin induced by femtosecond laser. To investigate the surface properties and functions of laser-processed CFRP, the roughness of laser-processed CFRP with typical surface structures and the surface wettability of CFRP processed by a femtosecond laser with different processing parameters were investigated, indicating increased roughness and excellent hydrophilicity (a contact angle as low as 28.1°) of femtosecond laser-processed CFRP. It will be conducive to the combination of CFRP with other materials or to reducing the friction resistance of CFRP used in medical implants. This work revealed the effect of femtosecond laser processing on the regulation of the physicochemical properties of CFRP, which can be applicable to the surface treatment and performance control of other fiber-resin composites.

METHODS

Femtosecond Laser Processing. The femtosecond laser used was a self-mode-locking Ti: Sapphire femtosecond laser was manufactured by Spectrum Physics company, which was mainly composed of a self-mode-locked oscillation stage (Tsunami) and a chirped pulse amplification stage (Spitfire Pro). The oscillation stage had a maximum laser output power of 560 mW and a repetition frequency of 80 MHz. After the amplification stage, the laser can be converted into a Gaussian linear polarized light with a maximum output power of 4.2 W. The central wavelength, pulse width, and repetition rate were 800 nm, 35 fs, and 1 kHz, respectively. The lightpath construction of the femtosecond laser processing system was reported in our previous study.[80] The plano-convex lens with a focal length of 100 mm was used to focus on the laser beam, and the laser spot diameter was about 16 μm. The range of the laser pulse energy was 0.5−50 μJ, the range of the laser scanning speed was 100−2000 μm/s, and the detailed values of the laser parameters are mentioned in the Figures and the illustration.

Characterization of the Surface Micro/Nanostructures of CFRP. Optical images were obtained by using an optical microscope (BX53) manufactured by the Olympus Corporation. SEM images were obtained using a field emission environmental scanning electron microscope (QUANTA 200 FEG) manufactured by the FEI Company. Raman spectra were obtained using a Raman spectrometer (inVia-Qontor) manufactured by Renishaw Company (532 nm light source, 50× focusing objective). XPS was performed using an X-ray photoelectron spectrometer (Quantera II) manufactured by ULVAC-PHI Corporation (Ar ion gun, calibration peak of binding energy was 284.6 eV). Surface roughness was tested with a three-dimensional laser confocal microscope (LEXT OLS4100) manufactured by the Olympus Corporation. The contact angle of water droplets on processed CFRP was tested by a Dataphysics video-based optical contact angle measuring instrument.

ASSOCIATED CONTENT

Supporting Information

The Supporting Information is available free of charge at https://pubs.acs.org/doi/10.1021/acsomega.4c00148.

Photograph of the used CFRP; measurement method of the diameter of carbon fibers; SEM image of CFRP by selectively laser etching at the selected location; morphology of laser-treated epoxy resin on CFRP; morphology of CFRP processed by femtosecond laser revealing the bamboo-like structures of carbon fibers; simple explanation for the decreasing diameter and more visible bamboo-like structure of carbon fibers with the increase of laser pulse energy; dependence of the diameter of carbon fibers on laser pulse energy; dependence of the diameter of carbon fibers on laser scanning speed; Raman frequencies (cm^{-1}) and assignments of the Raman modes of CFRP; complete parameters of surface roughness of the laser-processed CFRP with typical surface structures shown in Figure 5; comparison of wettability of surface-treated CFRP by different methods (PDF)

AUTHOR INFORMATION

Corresponding Author

Lan Jiang − *Laser Micro/Nano Fabrication Laboratory, School of Mechanical Engineering, Beijing Institute of Technology, Beijing 100081, China; Beijing Institute of Technology Chongqing Innovation Center, Chongqing 401120, China;* orcid.org/0000-0003-0488-1987; Email: jianglan@bit.edu.cn

Authors

Pei Zuo − *School of Mechanical and Electrical Engineering, Hubei Provincial Key Laboratory of Chemical Equipment Intensification and Intrinsic Safety, School of Optical Information and Energy Engineering, Wuhan Institute of Technology, Wuhan 430205, China;* orcid.org/0000-0002-3664-8787

Tongfeng Liu − *School of Mechanical and Electrical Engineering, Hubei Provincial Key Laboratory of Chemical Equipment Intensification and Intrinsic Safety, School of Optical Information and Energy Engineering, Wuhan Institute of Technology, Wuhan 430205, China*

Fang Li − *School of Mechanical and Electrical Engineering, Hubei Provincial Key Laboratory of Chemical Equipment Intensification and Intrinsic Safety, School of Optical Information and Energy Engineering, Wuhan Institute of Technology, Wuhan 430205, China;* orcid.org/0000-0002-5368-6291

Guoyan Wang − *Beijing Institute of Space Mechanics & Electricity, China Academy of Space Technology, Beijing 100094, China*

https://doi.org/10.1021/acsomega.4c00148
ACS Omega 2024, 9, 20988−20996

Kaihu Zhang − *Beijing Spacecrafts, China Academy of Space Technology, Beijing 100094, China*
Xin Li − *Laser Micro/Nano Fabrication Laboratory, School of Mechanical Engineering, Beijing Institute of Technology, Beijing 100081, China;* orcid.org/0000-0002-4743-5509
Weina Han − *Laser Micro/Nano Fabrication Laboratory, School of Mechanical Engineering, Beijing Institute of Technology, Beijing 100081, China;* orcid.org/0000-0002-2519-2104
Hong Tian − *School of Mechanical and Electrical Engineering, Hubei Provincial Key Laboratory of Chemical Equipment Intensification and Intrinsic Safety, School of Optical Information and Energy Engineering, Wuhan Institute of Technology, Wuhan 430205, China*
Lifei Hu − *School of Mechanical and Electrical Engineering, Hubei Provincial Key Laboratory of Chemical Equipment Intensification and Intrinsic Safety, School of Optical Information and Energy Engineering, Wuhan Institute of Technology, Wuhan 430205, China*
Helang Huang − *School of Mechanical and Electrical Engineering, Hubei Provincial Key Laboratory of Chemical Equipment Intensification and Intrinsic Safety, School of Optical Information and Energy Engineering, Wuhan Institute of Technology, Wuhan 430205, China*
Di Zhu − *School of Mechanical and Electrical Engineering, Hubei Provincial Key Laboratory of Chemical Equipment Intensification and Intrinsic Safety, School of Optical Information and Energy Engineering, Wuhan Institute of Technology, Wuhan 430205, China*

Complete contact information is available at: https://pubs.acs.org/10.1021/acsomega.4c00148

Author Contributions

The manuscript was written through contributions of all authors. All authors have given approval to the final version of the manuscript.

Notes

The authors declare no competing financial interest.

■ ACKNOWLEDGMENTS

This work was supported by the National Natural Science Foundation of China (U2037205, 52105427, 12374319, 52275401, 52350362, and 52005041), Hubei Provincial Natural Science Foundation of China (2023AFB648), Scientific Research Project of Hubei Provincial Department of Education (B2022055), Hubei Province Science and Technology Major Project (2022AAA008), Knowledge Innovation Program of Wuhan-Basic Research (2022010801010349), National Key R&D Program of China (2022YFB4602900), Chongqing Natural Science Foundation of China (cstc2021jcyj-cxttX0003 and CSTB2022NSCQ-MSX1322), Open Research Fund of State Key Laboratory of Transient Optics and Photonics (SKLST202206), and Science Foundation of Wuhan Institute of Technology (K202218).

■ REFERENCES

(1) Zhang, J.; Lin, G.; Vaidya, U.; Wang, H. Past, present and future prospective of global carbon fibre composite developments and applications. *Composites, Part B* **2023**, *250*, 110463.
(2) Zhao, M.; Wang, F.; Fu, R.; Sun, K.; Du, C.; Cui, J. Drilling study on CFRP/Al stack with different CFRP thickness using chip-breaking step drill bit. *J. Manuf. Process* **2023**, *90*, 300−309.
(3) Li, C.; Guo, L.; Lei, Y.; Gao, H.; Zio, E. A signal segmentation method for CFRP/CFRP stacks drilling-countersinking monitoring. *Mech. Syst. Signal Process.* **2023**, *196*, 110332.
(4) Hassan, M. H.; Abdullah, J.; Franz, G. Multi-Objective Optimization in Single-Shot Drilling of CFRP/Al Stacks Using Customized Twist Drill. *Materials* **2022**, *15*, 1981.
(5) Kamble, M.; Lakhnot, A. S.; Bartolucci, S. F.; Littlefield, A. G.; Picu, C. R.; Koratkar, N. Improvement in fatigue life of carbon fibre reinforced polymer composites via a Nano-Silica Modified Matrix. *Carbon* **2020**, *170*, 220−224.
(6) Kim, W.; Kim, Y. M.; Song, S.; Kim, E.; Kim, D.-G.; Jung, Y. C.; Yu, W.-R.; Na, W.; Choi, Y.-S. Manufacture of antibacterial carbon fiber-reinforced plastics (CFRP) using imine-based epoxy vitrimer for medical application. *Heliyon* **2023**, *9*, No. e16945.
(7) Chua, C. Y. X.; Liu, H.-C.; Di Trani, N.; Susnjar, A.; Ho, J.; Scorrano, G.; Rhudy, J.; Sizovs, A.; Lolli, G.; Hernandez, N. Carbon fiber reinforced polymers for implantable medical devices. *Biomaterials* **2021**, *271*, 120719.
(8) Saringer, W.; Nöbauer-Huhmann, I.; Knosp, E. Cranioplasty with Individual Carbon Fibre Reinforced Polymere (CFRP) Medical Grade Implants Based on CAD/CAM Technique. *Acta Neurochir.* **2002**, *144* (11), 1193−1203.
(9) Alvarez-Breckenridge, C.; Almeida, R. D.; Haider, A.; Muir, M.; Bird, J.; North, R.; Rhines, L.; Tatsui, C. Carbon Fiber-Reinforced Polyetheretherketone Spinal Implants for Treatment of Spinal Tumors: Perceived Advantages and Limitations. *Neurospine* **2023**, *20*, 317−326.
(10) Früh, H. J.; Liebetrau, A.; Bertagnoli, R. [Fusion implants of carbon fiber reinforced plastic]. *Orthopade* **2002**, *31*, 454−458.
(11) Zhou, H.; Su, Y.; Zhang, J.; Li, H.; Zhou, L.; Huang, H. A novel embedded all-solid-state composite structural supercapacitor based on activated carbon fiber electrode and carbon fiber reinforced polymer matrix. *Chem. Eng. J.* **2023**, *454*, 140222.
(12) Zhou, H.; Duongthipthewa, A.; Zhang, J.; Li, H.; Peng, L.; Fu, Y.; Huang, H.; Zhou, L. A composite structural supercapacitor based on Ni−Co-layered double hydroxide−coated carbon cloth electrodes. *Compos. Sci. Technol.* **2023**, *240*, 110068.
(13) Pernice, M. F.; Qi, G.; Senokos, E.; Anthony, D. B.; Nguyen, S.; Valkova, M.; Greenhalgh, E. S.; Shaffer, M. S. P.; Kucernak, A. R. J. Mechanical, electrochemical and multifunctional performance of a CFRP/carbon aerogel structural supercapacitor and its corresponding monofunctional equivalents. *Multifunct. Mater.* **2022**, *5*, 025002.
(14) Li, W.; Rong, Y.; Huang, Y.; Chen, L.; Yang, Z.; Zhang, G. Effect of thermal damage on dynamic and static mechanical properties of CFRP short pulse laser hole cutting. *Eng. Fract. Mech.* **2023**, *286*, 109306.
(15) Kim, D.-G.; Yang, S.-H. Efficient Analysis of CFRP Cutting Force and Chip Formation Based on Cutting Force Models Under Various Cutting Conditions. *Int. J. Precis Eng. Manuf.* **2023**, *24* (7), 1235−1251.
(16) Xu, J.; Geier, N.; Shen, J.; Krishnaraj, V.; Samsudeensadham, S. A review on CFRP drilling: Fundamental mechanisms, damage issues, and approaches toward high-quality drilling. *J. Mater. Res. Technol.* **2023**, *24*, 9677−9707.
(17) Oliveira, V.; Moreira, R. D. F.; de Moura, M. F. S. F.; Vilar, R. Surface patterning of CRFP composites using femtosecond laser interferometry. *Appl. Phys. A: Mater. Sci. Process.* **2018**, *124*, 231.
(18) Moreira, R. D. F.; Oliveira, V.; Silva, F. G. A.; Vilar, R.; de Moura, M. F. S. F. Influence of femtosecond laser treated surfaces on the mode I fracture toughness of carbon-epoxy bonded joints. *Int. J. Adhes. Adhes.* **2018**, *82*, 108−113.
(19) Moreira, R. D. F.; Oliveira, V.; Silva, F. G. A.; Vilar, R.; de Moura, M. F. S. F. Mode II fracture toughness of carbon−epoxy bonded joints with femtosecond laser treated surfaces. *Int. J. Mech Sci.* **2018**, *148*, 707−713.
(20) Oliveira, V.; Sharma, S. P.; de Moura, M. F. S. F.; Moreira, R. D. F.; Vilar, R. Surface treatment of CFRP composites using femtosecond laser radiation. *Opt. Lasers Eng.* **2017**, *94*, 37−43.

(21) Park, S.-M.; Roy, R.; Kweon, J.-H.; Nam, Y. Strength and failure modes of surface treated CFRP secondary bonded single-lap joints in static and fatigue tensile loading regimes. *Composites, Part A* **2020**, *134*, 105897.
(22) Rauh, B.; Kreling, S.; Kolb, M.; Geistbeck, M.; Boujenfa, S.; Suess, M.; Dilger, K. UV-laser cleaning and surface characterization of an aerospace carbon fibre reinforced polymer. *Int. J. Adhes. Adhes.* **2018**, *82*, 50−59.
(23) Yu, B.; He, P.; Jiang, Z.; Yang, J. Interlaminar fracture properties of surface treated Ti-CFRP hybrid composites under long-term hygrothermal conditions. *Composites, Part A* **2017**, *96*, 9−17.
(24) Wang, Z.; Ma, Y.; Yuan, B.; Wu, C.; Li, C.; Sun, S. Development of Laser Processing Carbon-Fiber-Reinforced Plastic. *Sensors* **2023**, *23*, 3659.
(25) Wingfield, J. R. J. Treatment of composite surfaces for adhesive bonding. *Int. J. Adhes. Adhes.* **1993**, *13*, 151−156.
(26) Ledesma, R. I.; Palmieri, F. L.; Lin, Y.; Belcher, M. A.; Ferriell, D. R.; Thomas, S. K.; Connell, J. W. Picosecond laser surface treatment and analysis of thermoplastic composites for structural adhesive bonding. *Compos B Eng.* **2020**, *191*, 107939.
(27) Li, C.; Viswanathan-Chettiar, S.; Sun, F.; Shi, Z.; Blackman, B. Effect of CFRP surface topography on the adhesion and strength of composite-composite and composite-metal joints. *Composites, Part A* **2023**, *164*, 107275.
(28) Qi, L.; Min, W.; Gao, R.; Li, Z.; Yu, M.; Sun, Z. Optimization of interfacial bonding properties between thermoplastic liners and carbon fiber-reinforced composites by atmospheric-pressure plasma and failure mechanism study. *Polym. Compos.* **2023**, *44*, 2361−2378.
(29) Wang, D.; Li, Y.; Zou, T.; Fu, J.; Liu, Z. Increasing strength and fracture toughness of carbon fibre-reinforced plastic adhesively bonded joints by combining peel-ply and oxygen plasma treatments. *Appl. Surf. Sci.* **2023**, *612*, 155768.
(30) Kim, W.-J.; Heo, Y.-J.; Lee, J.-H.; Rhee, K. Y.; Park, S.-J. Effect of Atmospheric-Pressure Plasma Treatments on Fracture Toughness of Carbon Fibers-Reinforced Composites. *Molecules* **2021**, *26*, 3698.
(31) Encinas, N.; Oakley, B. R.; Belcher, M. A.; Blohowiak, K. Y.; Dillingham, R. G.; Abenojar, J.; Martínez, M. A. Surface modification of aircraft used composites for adhesive bonding. *Int. J. Adhes. Adhes.* **2014**, *50*, 157−163.
(32) Çoban, O.; Akman, E.; Bora, M. Ö.; Genc Oztoprak, B.; Demir, A. Laser surface treatment of CFRP composites for a better adhesive bonding owing to the mechanical interlocking mechanism. *Polym. Compos.* **2019**, *40*, 3611−3622.
(33) Wang, F.; Bu, H.; Ma, W.; Zhang, P.; Zhan, X. Influence of the different surface treatments on fracture property of CFRP adhesive joint. *J. Adhes. Sci. Technol.* **2023**, *37*, 961−975.
(34) Veltrup, M.; Lukasczyk, T.; Mayer, B. Effect of re-depositions and fiber exposure on the adhesive bond strength of CFRP after UV excimer laser treat.ment. *Appl. Phys. A: Mater. Sci. Process.* **2022**, *128*, 786.
(35) Li, H.; Liu, H.; Li, S.; Zhao, Q.; Qin, X. Influence of high pulse fluence infrared laser surface pretreatment parameters on the mechanical properties of CFRP/aluminium alloy adhesive joints. *J. Adhes.* **2023**, *99*, 584−605.
(36) Jiang, L.; Wang, A.-D.; Li, B.; Cui, T.-H.; Lu, Y.-F. Electrons dynamics control by shaping femtosecond laser pulses in micro/nanofabrication: modeling, method, measurement and application. *Light: Sci. Appl.* **2018**, *7*, 17134.
(37) Zuo, P.; Jiang, L.; Li, X.; Tian, M.; Xu, C.; Yuan, Y.; Ran, P.; Li, B.; Lu, Y. Maskless Micro/Nanopatterning and Bipolar Electrical Rectification of MoS2 Flakes Through Femtosecond Laser Direct Writing. *ACS Appl. Mater. Interfaces* **2019**, *11*, 39334−39341.
(38) Zuo, P.; Jiang, L.; Li, X.; Ran, P.; Li, B.; Song, A.; Tian, M.; Ma, T.; Guo, B.; Qu, L.; et al. Enhancing charge transfer with foreign molecules through femtosecond laser induced MoS2 defect sites for photoluminescence control and SERS enhancement. *Nanoscale* **2019**, *11*, 485−494.
(39) Zuo, P.; Jiang, L.; Li, X.; Li, B.; Xu, Y.; Shi, X.; Ran, P.; Ma, T.; Li, D.; Qu, L.; et al. Shape-Controllable Gold Nanoparticle−MoS 2 Hybrids Prepared by Tuning Edge-Active Sites and Surface Structures of MoS 2 via Temporally Shaped Femtosecond Pulses. *ACS Appl. Mater. Interfaces* **2017**, *9*, 7447−7455.
(40) Huang, Y.; Xie, X.; Li, M.; Xu, M.; Long, J. Copper circuits fabricated on flexible polymer substrates by a high repetition rate femtosecond laser-induced selective local reduction of copper oxide nanoparticles. *Opt. Express* **2021**, *29*, 4453−4463.
(41) Zhang, D.; Li, X.; Fu, Y.; Yao, Q.; Li, Z.; Sugioka, K. Liquid vortexes and flows induced by femtosecond laser ablation in liquid governing formation of circular and crisscross LIPSS. *Opto-Electron. Adv.* **2022**, *5*, 210066.
(42) Saraj, C. S.; Singh, S. C.; Verma, G.; Rajan, R. A.; Li, W.; Guo, C. Laser-induced periodic surface structured electrodes with 45% energy saving in electrochemical fuel generation through field localization. *Opto-Electron. Adv.* **2022**, *5*, 210105.
(43) Qian, X.; Wang, X.; Zhong, J.; Zhi, J.; Heng, F.; Zhang, Y.; Song, S. Effect of fiber microstructure studied by Raman spectroscopy upon the mechanical properties of carbon fibers. *J. Raman Spectrosc.* **2019**, *50*, 665−673.
(44) Wu, T.; Lu, C.; Sun, T.; Li, Y. Study on Raman multi-peak fitting and structure quantitative analysis of PAN-based carbon fibers. *J. Mater. Sci.* **2022**, *57*, 15385−15412.
(45) Sadezky, A.; Muckenhuber, H.; Grothe, H.; Niessner, R.; Pöschl, U. Raman microspectroscopy of soot and related carbonaceous materials: Spectral analysis and structural information. *Carbon* **2005**, *43*, 1731−1742.
(46) Deng, J.; Xu, L.; Liu, J.; Peng, J.; Han, Z.; Shen, Z.; Guo, S. Efficient method of recycling carbon fiber from the waste of carbon fiber reinforced polymer composites. *Polym. Degrad. Stab.* **2020**, *182*, 109419.
(47) Zhang, R. L.; Gao, B.; Ma, Q. H.; Zhang, J.; Cui, H. Z.; Liu, L. Directly grafting graphene oxide onto carbon fiber and the effect on the mechanical properties of carbon fiber composites. *Mater. Des.* **2016**, *93*, 364−369.
(48) Pollock, N.; Fowler, G.; Twyman, L. J.; McArthur, S. L. Synthesis and characterization of immobilized PAMAM dendrons. *Chem. Commun.* **2007**, 24822484. .
(49) Yan, H.; Lu, C.-X.; Jing, D.-Q.; Chang, C.-B.; Liu, N.-X.; Hou, X.-L. Recycling of carbon fibers in epoxy resin composites using supercritical 1-propanol. *New Carbon Mater.* **2016**, *31*, 46−54.
(50) Solomon, J. L.; Madix, R. J.; Stöhr, J. Orientation and absolute coverage of benzene, aniline, and phenol on Ag(110) determined by NEXAFS and XPS. *Surf. Sci.* **1991**, *255*, 12−30.
(51) Ji, F.; Liu, C.; Hu, Y.; Xu, S.; He, Y.; Zhou, J.; Zhang, Y. Chemically Grafting Carbon Nanotubes onto Carbon Fibers for Enhancing Interfacial Properties of Fiber Metal Laminate. *Materials* **2020**, *13*, 3813.
(52) Sandomierski, M.; Strzemiecka, B.; Chehimi, M. M.; Voelkel, A. Reactive Diazonium-Modified Silica Fillers for High-Performance Polymers. *Langmuir* **2016**, *32*, 11646−11654.
(53) Lau, W. M.; Huang, L. J.; Bello, I.; Yiu, Y. M.; Lee, S. T. Modification of surface band bending of diamond by low energy argon and carbon ion bombardment. *J. Appl. Phys.* **1994**, *75*, 3385−3391.
(54) Morar, J. F.; Himpsel, F. J.; Hollinger, G.; Jordan, J. L.; Hughes, G.; McFeely, F. R. C 1s excitation studies of diamond (111). I. Surface core levels. *Phys. Rev. B* **1986**, *33*, 1340.
(55) Clark, D. T.; Adams, D. B.; Dilks, A.; Peeling, J.; Thomas, H. R. Some aspects of shake-up phenomena in some simple polymer systems. *J. Electron Spectrosc. Relat. Phenom.* **1976**, *8*, 51−60.
(56) Peeling, J.; Clark, D. T. An ESCA study of the photo-oxidation of the surface of polystyrene film. *Polym. Degrad. Stab.* **1981**, *3*, 97−105.
(57) Wang, L.; Yin, K.; Deng, Q.; Huang, Q.; He, J.; Duan, J.-A. Wetting Ridge-Guided Directional Water Self-Transport. *Adv. Sci.* **2022**, *9*, 2204891.
(58) He, Y.; Wang, L.; Wu, T.; Wu, Z.; Chen, Y.; Yin, K. Facile fabrication of hierarchical textures for substrate-independent and durable superhydrophobic surfaces. *Nanoscale* **2022**, *14*, 9392−9400.

https://doi.org/10.1021/acsomega.4c00148
ACS Omega 2024, 9, 20988−20996

(59) Huang, Q.; Yin, K.; Wang, L.; Deng, Q.; Arnusch, C. J. Femtosecond laser-scribed superhydrophilic/superhydrophobic self-splitting patterns for one droplet multi-detection. *Nanoscale* **2023**, *15*, 11247−11254.
(60) Deng, Q.; Yin, K.; Wang, L.; Zhang, H.; Huang, Q.; Luo, Z.; He, J.; Duan, J.-A. One Droplet toward Efficient Alcohol Detection Using Femtosecond Laser Textured Micro/Nanostructured Surface with Superwettability. *Small Methods* **2023**, *7*, 2300290.
(61) Long, J.; Zhou, P.; Huang, Y.; Xie, X. Enhancing the Long-Term Robustness of Dropwise Condensation on Nanostructured Superhydrophobic Surfaces by Introducing 3D Conical Microtextures Prepared by Femtosecond Laser. *Adv. Mater. Interfaces* **2020**, *7*, 2000997.
(62) Long, J.; Weng, Q.; Hong, W.; Cao, Z.; Zhou, P.; Xie, X. Fast water flow in laser micromachined microgrooves with nonuniform surface wettability. *Exp. Therm. Fluid Sci.* **2019**, *103*, 9−17.
(63) Vorobyev, A. Y.; Guo, C. Direct femtosecond laser surface nano/microstructuring and its applications. *Laser Photonics Rev.* **2013**, *7*, 385−407.
(64) Rajan, R. A.; Ngo, C.-V.; Yang, J.; Liu, Y.; Rao, K. S.; Guo, C. Femtosecond and picosecond laser fabrication for long-term super-hydrophilic metal surfaces. *Opt. Laser Technol.* **2021**, *143*, 107241.
(65) Xie, X.; Weng, Q.; Luo, Z.; Long, J.; Wei, X. Thermal performance of the flat micro-heat pipe with the wettability gradient surface by laser fabrication. *Int. J. Heat Mass Transf* **2018**, *125*, 658−669.
(66) Tan, J.; Liu, W.; Wang, Z. Hydrophobic epoxy resins modified by low concentrations of comb-shaped fluorinated reactive modifier. *Prog. Org. Coat.* **2017**, *105*, 353−361.
(67) Yu, M.; Chen, Z.; Li, J.; Tan, J.; Zhu, X. High-Branched Organosilicon Epoxy Resin with Low Viscosity, Excellent Toughness, Hydrophobicity, and Dielectric Property. *Molecules* **2023**, *28*, 2826.
(68) Fan, F.; Li, F.-X.; Tian, S.-C.; Sheng, M.; Khan, W.; Shi, A.-P.; Zhou, Y.; Xu, Q. Hydrophobic epoxy resin coated proppants with ultra-high self-suspension ability and enhanced liquid conductivity. *Pet. Sci.* **2021**, *18*, 1753−1759.
(69) İplikçi, H.; Barisik, M.; Türkdoğan, C.; Martin, S.; Yeke, M.; Nuhoğlu, K.; Esenoğlu, G.; Tanoğlu, M.; Aktaş, E.; Dehneliler, S.; et al. Effects of nanosecond laser ablation parameters on surface modification of carbon fiber reinforced polymer composites. *J. Compos Mater.* **2023**, *57*, 2843−2855.
(70) Yang, C.; Chao, J.; Zhang, J.; Zhang, Z.; Liu, X.; Tian, Y.; Zhang, D.; Chen, F. Functionalized CFRP surface with water-repellence, self-cleaning and anti-icing properties. *Colloids Surf., A* **2020**, *586*, 124278.
(71) Kumar, D.; Liedl, G.; Gururaja, S. Formation of sub-wavelength laser induced periodic surface structure and wettability transformation of CFRP laminates using ultra-fast laser. *Mater. Lett.* **2020**, *276*, 128282.
(72) Zhang, Z.; Zhou, J.; Ren, Y.; Li, W.; Li, S.; Chai, N.; Zeng, Z.; Chen, X.; Yue, Y.; Zhou, L.; et al. Passive Deicing CFRP Surfaces Enabled by Super-Hydrophobic Multi-Scale Micro-Nano Structures Fabricated via Femtosecond Laser Direct Writing. *Nanomaterials* **2022**, *12*, 2782.
(73) Qiu, S.; Fuentes, C. A.; Zhang, D.; Van Vuure, A. W.; Seveno, D. Wettability of a Single Carbon Fiber. *Langmuir* **2016**, *32*, 9697−9705.
(74) Zhang, J.; Jia, K.; Huang, Y.; Liu, X.; Xu, Q.; Wang, W.; Zhang, R.; Liu, B.; Zheng, L.; Chen, H.; et al. Intrinsic Wettability in Pristine Graphene. *Adv. Mater.* **2022**, *34*, 2103620.
(75) Kvashnin, A. G.; Chernozatonskii, L. A.; Yakobson, B. I.; Sorokin, P. B. Phase Diagram of Quasi-Two-Dimensional Carbon, From Graphene to Diamond. *Nano Lett.* **2014**, *14*, 676−681.
(76) Jayasundara, D. R.; Cullen, R. J.; Colavita, P. E. In Situ and Real Time Characterization of Spontaneous Grafting of Aryldiazonium Salts at Carbon Surfaces. *Chem. Mater.* **2013**, *25*, 1144−1152.
(77) Duan, Z.; Zhu, Y.; Ren, P.; Jia, J.; Yang, S.; Zhao, G.; Xie, Y.; Zhang, J. Non-UV activated superhydrophilicity of patterned Fe-doped TiO2 film for anti-fogging and photocatalysis. *Appl. Surf. Sci.* **2018**, *452*, 165−173.
(78) Kurihara, K.; Hokari, R.; Takada, N. Capillary Effect Enhancement in a Plastic Capillary Tube by Nanostructured Surface. *Polymers* **2021**, *13*, 628.
(79) Cheng, S.; Ma, J.; Gong, F.; Shen, J. Thermoplastic Forming of a Hydrophilic Surface with a Nanostructure Array on Zr-Cu-Ni-Al-Y Bulk Metallic Glass. *Metals* **2021**, *11*, 1520.
(80) Zuo, P.; Jiang, L.; Li, X.; Tian, M.; Yuan, Y.; Han, W.; Ma, L.; Hu, L.; He, Z.; Li, F. MoS_2 core-shell nanoparticles prepared through liquid-phase ablation and light exfoliation of femtosecond laser for chemical sensing. *Sci. China: Technol. Sci.* **2023**, *66*, 853−862.

https://doi.org/10.1021/acsomega.4c00148
ACS Omega 2024, 9, 20988−20996